

Investigating magnetic activity cycles in solar-like oscillators using asteroseismic data from the K2 mission

Gleb Berloff¹ , Anne-Marie Broomhall^{2*} , George T. Hookway³ , Mikkel N. Lund⁴ ,
 Laura Jade Millson² , and Dmitrii Kolotkov^{2,5} 

¹*Department of Physics, University of Warwick, Coventry, CV4 7AL, UK*

²*Centre for Fusion, Space and Astrophysics, University of Warwick, Coventry, CV4 7AL, UK*

³*School of Physics and Astronomy, University of Birmingham, Edgbaston, Birmingham, B15 2TT, UK*

⁴*Stellar Astrophysics Centre, Department of Physics and Astronomy, Aarhus University, Ny Munkegade 120, 8000, Aarhus C, Denmark*

⁵*Engineering Research Institute “Ventspils International Radio Astronomy Centre (VIRAC)”, Ventspils University of Applied Sciences, Ventspils, LV-3601, Latvia*

Accepted XXX. Received YYY; in original form ZZZ

ABSTRACT

We present the results of an investigation into the possible presence of magnetic activity cycles in stars observed in two observational campaigns by the K2 mission. This study was based on the KEYSTONE asteroseismic sample of solar-like oscillators, which contained 20 stars for which we were able to determine whether the asteroseismic p-mode frequencies varied in time. These frequency shifts ($\delta\nu$) were determined using a cross-correlation method and using the individual mode frequencies, obtained by fitting power spectra. Three stars were found to exhibit $\delta\nu$ larger than their associated errors ($\sigma_{\delta\nu}$) using both methods, while two more stars exhibited $\delta\nu > \sigma_{\delta\nu}$ when the cross correlation was used and a further two stars exhibited $\delta\nu > \sigma_{\delta\nu}$ when the fitted frequencies were used. When considering the whole sample of 20 stars, the amplitude of $\delta\nu$ showed no dependence on the large frequency separation and metallicity. However, $\delta\nu$ was observed to increase with rotation rate and effective temperature. Our sample contained a number of evolved subgiant stars, allowing us to expand the parameter space usually considered when comparing $\delta\nu$ with stellar parameters. While $\delta\nu$ was small for all of the evolved stars, one was found to have $\delta\nu > \sigma_{\delta\nu}$, raising the possibility that these evolved stars may still exhibit variable magnetic activity.

Key words: asteroseismology – stars: activity – stars: magnetic field

1 Introduction

Sunspots are pronounced dark features on the surface of the Sun associated with colder-than-average temperatures in the solar photosphere. In 1843, following an anomalous 75-year period in the 17th-18th century in which almost no sunspots were observed, an era known as the Maunder minimum (see e.g. Hathaway 2015, and references therein), Heinrich Schwabe discovered that the amount of sunspots visible on the surface of the Sun typically varies with an approximate 11-year periodicity (Schwabe 1844). The beginning of each sunspot cycle is indicated by sunspots appearing at mid-latitudes, after which they are observed at latitudes increasingly close to the equator, forming what is now known as the butterfly diagram (Maunder 1904; Hathaway 2015). The first association that sunspots are related to magnetic activity was made by Hale (1908), who discovered that sunspots typically arose in pairs of opposite magnetic polarity, and that the apparent solar sunspot cycle of 11 years is related to a magnetic activity cycle, with a period of 22 years (Balogh & Thompson 2009). The magnetic cycle of the Sun is now modelled via a magnetic dynamo typically thought to arise due to turbulent shearing flows in the convective zone of the Sun, although there are still many outstanding questions about exactly how and why the magnetic field of the Sun arises (Charbonneau 2014).

Considering that stars are located significantly further away than the Sun, and as such, direct observations of starspots are

impractical, many other methods have been devised to infer the presence of activity cycles in other stars. For example, chromospheric indicators of activity have been observed on other stars, most notably as part of the Mount Wilson survey (Baliunas et al. 1995). Solar values of these activity proxies are known to correlate well with sunspot observations (Ferreira et al. 2024). The Mount Wilson survey revealed the existence of magnetic activity cycles in other stars that, for a single polarity change (akin to our 11 yr solar cycle), ranged between 1 yr and 21 yrs. By studying and analysing the magnetic activity cycles or their indicators in other stars, it is hoped, among other aspects, to formalise constraints on existing dynamo models of stellar magnetic cycles over a broader parameter range. In this study, we use an alternative proxy of stellar activity based upon observations of stellar oscillations.

Observations of the Sun have long suggested that as the activity of the star increases, the frequencies of the p-mode oscillations also increase (Woodard & Noyes 1985; Elsworth et al. 1990; Broomhall et al. 2014, and references therein). The change in frequency of p modes as a function of time is known as the frequency shift, $\delta\nu$. Observed frequency shifts are commonly thought to be caused either directly by magnetic fields (with the Lorentz force providing a restoring force that leads to an increase in the mode frequency) or via indirect effects, which occur because the magnetic field changes the internal stratification of the star. It is not yet clear which of these effects dominate (e.g. Dziembowski & Goode 2005; Kiefer & Roth 2018; Kolotkov et al. 2024).

* E-mail: a-m.broomhall@warwick.ac.uk

The first asteroseismic evidence for a magnetic activity cycle on a star other than the Sun was on HD 49933, which was observed by the CoRoT mission (García et al. 2010). The same behaviour has now been detected in other stars (see Jeffers et al. 2023 for a recent review), most notably stars observed by NASA’s Kepler mission (Borucki et al. 2010). In fact, there are now sufficient observations of frequency shifts on stars that it has been possible to investigate how the amplitude of these frequency shifts, and by inference the amplitudes of stellar cycles, may relate to different stellar parameters. Santos et al. (2019) compared p-mode frequency shifts detected on 75 stars observed by Kepler to various stellar parameters, finding that the amplitude of the frequency shift correlated positively with the chromospheric activity indicator R_{HK} and rotation rate, and was anti-correlated with stellar age. Santos et al. also noticed a positive correlation with effective temperature and postulated that this was because the hotter a star, the more sensitive the p modes are to any magnetic perturbations, in agreement with predictions made by Metcalfe et al. (2007) and Kiefer et al. (2019). However, it must be remembered that even for stars observed during the full ≈ 4 years of the Kepler mission, the observations may not cover a full stellar cycle.

Kepler stared at one patch of the sky for the entirety of its nominal mission (2009–2013). However, when Kepler was no longer able to maintain stable pointing, it was repurposed as K2 (Howell et al. 2014), which operated between 2014 and 2018. Unlike Kepler, K2 changed its field of view regularly and made photometric observations of stars in specified areas along the ecliptic, referred to as “campaigns”. The standard duration of a K2 campaign was just 80 days, which is not sufficient to determine frequency shifts alone. However, some of the campaigns overlapped, meaning that certain stars were observed in multiple non-consecutive campaigns by K2. Therefore, this study aims to detect frequency shifts and, by inference, magnetic activity cycles, by comparing asteroseismic observations in two different K2 campaigns. Although with only two data points we cannot determine whether any detected shifts represent activity cycles, this study highlights stars worthy of further observation and contributes to our understanding of which stellar parameters play a role in determining the amplitude of activity variations.

Since we aim to detect evidence for magnetic activity using variations in p-mode frequencies, our focus is on solar-like oscillators. Previous works, such as Santos et al. (2018), have concentrated only on main-sequence solar-like oscillators. However, subgiants (and red giants) are also solar-like oscillators, and we include several subgiants in our sample. While these older stars are not expected to be as magnetically active as their main sequence counterparts (Skumanich 1972; Mamajek & Hillenbrand 2008), Kiefer & Broomhall (2020) predicted that evolved stars may be more sensitive to any magnetic field and so we also include subgiants in our sample, expanding the parameter space considered by Santos et al. (2018, 2019). Kjeldsen et al. (2025) used asteroseismology to study a subgiant star, β Aql, which appears to have a 4.7 ± 0.4 yr activity cycle, but found no significant change in frequency between the years 2022 and 2023. This work also represents an extension to González-Cuesta et al. (2023) who performed an asteroseismic study of eight stars from K2 campaigns 6 and 17. Here, we do not restrict our study to just these two campaigns; therefore, we expand upon their sample of stars.

The remainder of the paper is structured as follows. In Section 2 we describe our sample of stars, the data used and the methods by which the frequency shifts were determined. Section 3 contains the main results including a comparison of the observed frequency shifts with various stellar parameters, put into context by comparison with those found by Santos et al. (2019). Section 4 contains our main conclusions.

2 Method of research

2.1 Identification of target stars

Lund et al. (2024) recently published the K2 asteroseismic KEYSTONE sample of 173 dwarf and subgiant stars that exhibited solar-like oscillations in power spectra constructed from short-cadence K2 data prepared for asteroseismic analyses by the K2P² pipeline (Handberg & Lund 2014; Lund et al. 2015). We identified the stars in the KEYSTONE sample that were observed in two K2 campaigns and used the data prepared using the K2P² pipeline to determine whether any change in oscillation frequency was observed between campaigns: Two methods were used to determine the observed frequency shifts and these will be described in Sections 2.3 and 2.4. Lund et al. (2024) identified 30 stars that were observed in multiple campaigns, however, for 9 stars, their Table 4 only provides values of $\Delta\nu$ and ν_{max} for single campaigns and/or when the data from the campaigns were combined. This was because the signal to noise in one of the campaigns was not sufficient on its own to obtain these parameters. We therefore excluded those stars from our study. Additionally, we found that for EPIC 24630350, the p-mode signal to noise was not sufficient to allow the frequency shifts to be determined. In total, we identified 20 stars that were observed in more than one campaign and were suitable for this study. We now provide further details on the stars in our sample.

2.2 Parameters of stars in our sample

Values of the large separation ($\Delta\nu$, which is the frequency spacing between neighbouring radial orders, n , for modes of the same angular degree, ℓ) and the frequency of maximum p mode power (ν_{max} , which is generally measured as the centre of a Gaussian fitted to the acoustic modes) for the 20 stars considered in our sample are given in Table 1. The values of $\Delta\nu$ and ν_{max} , which were incorporated into our method for determining the frequency shifts, were obtained from Lund et al. (2024). In Lund et al., three different methods were used to obtain values for these global asteroseismic parameters. Here we quote the coefficient of variation values, obtained using the method described in Bell et al. (2019). In Section 3, we compare the obtained frequency shifts to various stellar parameters. The stellar parameters considered include: $\Delta\nu$; effective temperature (T_{eff}); surface gravity ($\log g$); metallicity ($[\text{Fe}/\text{H}]$); and rotation period (P_{rot}). For our sample, the values of these parameters were also obtained from Lund et al. and are included in Table 1. We note that Lund et al. gave values for the projected rotational velocity, $\nu \sin i$, rather than P_{rot} . We therefore derived P_{rot} from $\nu \sin i$, taking $i = 90^\circ$, meaning the values given in Table 1 represent an upper estimate. When converting from $\nu \sin i$ to rotation period, we calculated radius values using the asteroseismic scaling relations (e.g. García & Ballot 2019).

2.3 Determination of oscillation frequency shifts using cross correlations

Frequency shifts ($\delta\nu$) were determined using the cross-correlation technique described in Kiefer et al. (2017). The process is summarised here for clarity. For each star and each campaign, a power spectrum was obtained from the K2P² cleaned data using a Lomb-Scargle periodogram. It was important when determining the cross correlation that the power spectra were evaluated at the same frequency locations. Therefore, the frequency array used to evaluate the power spectrum for the first campaign was also used to determine the power spectrum for the second campaign.

Using values of ν_{max} and $\Delta\nu$ from Table 1, the cross-correlation was determined over a range of $\nu_{\text{max}} \pm 4\Delta\nu$. This range will contain approximately eight overtones for each angular degree that have

Table 1. Stellar parameters for stars in the KEYSTONE sample observed by multiple K2 campaigns. Values were obtained from Lund et al. (2024). The uncertainty on all metallicity ([Fe/H]) values was 0.101 dex, while the error on all surface gravity ($\log g$) values was 0.1 dex.

EPIC	$\Delta\nu$ (μHz)	ν_{max} (μHz)	T_{eff} (K)	$\log g$ (cgs;dex)	[Fe/H] (dex)	P_{rot} (d)
211403248	21.5 \pm 0.5	335 \pm 7	5020 \pm 40	3.4	0.009	62 \pm 8
211409560	19.2 \pm 0.4	271 \pm 7	4980 \pm 40	3.4	-0.024	66 \pm 10
212485100	87.4 \pm 0.6	1803 \pm 21	6100 \pm 40	4.2	-0.038	12.8 \pm 1.0
212487676	76.5 \pm 0.6	1441 \pm 15	6020 \pm 50	4.1	-0.313	18.8 \pm 2.1
212617037	51.0 \pm 0.5	886 \pm 28	6570 \pm 50	3.9	0.012	3.56 \pm 0.13
212683142	45.7 \pm 0.5	798 \pm 10	5920 \pm 40	3.9	-0.051	25.0 \pm 2.5
212708252	132.3 \pm 0.8	2890 \pm 29	5550 \pm 30	4.4	-0.094	53 \pm 19
212709737	78.1 \pm 0.5	1640 \pm 37	6560 \pm 50	4.2	-0.139	6.40 \pm 0.28
212772187	87.9 \pm 0.6	1846 \pm 40	6470 \pm 50	4.2	-0.046	5.89 \pm 0.26
245961434	47.3 \pm 0.5	808 \pm 12	5980 \pm 40	3.9	-0.007	16.2 \pm 1.2
245972483	85.0 \pm 0.6	1793 \pm 16	6130 \pm 40	4.2	-0.204	10.0 \pm 0.6
246154489	14.4 \pm 0.4	189 \pm 3	4950 \pm 30	3.2	-0.366	89 \pm 14
246212144	53.4 \pm 0.4	979 \pm 17	6370 \pm 50	4.0	-0.040	11.1 \pm 0.6
212478598	35.7 \pm 0.6	528 \pm 5	5050 \pm 30	3.6	-0.356	57 \pm 11
212509747	66.4 \pm 0.5	1306 \pm 19	6420 \pm 40	4.1	-0.266	13.5 \pm 0.9
246134147	83.6 \pm 0.6	1727 \pm 22	6240 \pm 50	4.2	-0.366	10.1 \pm 0.6
246033065	102.0 \pm 0.7	2320 \pm 50	4130 \pm 30	4.3	-0.096	9.2 \pm 0.6
246438837	55.7 \pm 0.5	1071 \pm 17	6160 \pm 40	4.0	0.005	12.4 \pm 0.7
212516207	68.3 \pm 0.5	1398 \pm 18	6150 \pm 50	4.1	0.132	15.0 \pm 1.1
246305274	46.7 \pm 0.5	799 \pm 13	6210 \pm 40	3.9	-0.416	14.8 \pm 1.0

the highest signal to noise, which is sufficient to determine the frequency shift. A wider range runs the risk of incorporating low signal-to-noise p modes. The left-hand panel of Figure 1 shows examples of the spectra over this frequency range that were observed for EPIC 212509747. The cross correlation between these spectra was determined, and the location of the central peak in the cross correlation then corresponds to the change in frequency between the oscillations in the two campaigns. However, since the data in the cross correlation are correlated with each other, rather than fitting the cross correlation itself, 1000 realisations of the power spectra from each campaign were simulated. The realisations were simulated by first smoothing the power spectra obtained from the raw data, using a boxcar smoothing. The smoothed power spectra can be thought of as representing the underlying signal in the data and should, therefore, capture the relatively sharp structure of the p-mode peaks while smoothing out the noise. The width and separation of the mode peaks varied across the sample due to the range of stellar parameters (e.g. T_{eff} , $\log g$) considered. Therefore, the smoothing window, n_{sm} , was taken to be the maximum of the integer number of frequency bins closest to $0.05\Delta\nu$ or five frequency bins. Following a visual inspection, this was found to represent a good balance between smoothing the noise, while maintaining the structure of the p-mode peaks. A lower limit of five frequency bins was put in place as anything below this would not sufficiently smooth the noise to reveal the signal from the p-mode peaks. For EPIC 212509747 this corresponded to a smoothing width of $n_{\text{sm}} = 22$ bins or 3.2 μHz . Although we note that conversion between bins and frequency will vary slightly from star to star, depending on the frequency resolution of the computed Lomb-Scargle periodogram. The square root of the smoothed power spectra was then determined to produce amplitude spectra. We then generated independent ‘real’ and ‘imaginary’ realisations by multiplying the amplitude spectra by arrays of Gaussian distributed random noise, with a mean of zero and standard deviation of unity (see e.g. Kiefer et al. 2017). The real and imaginary realisation components were then recombined to form a single power spectrum realisation. Realisations were created for each campaign, and the cross correlation of the realisations was determined (see Figure 1). The central peak was fitted with a Lorentzian curve over a range of $0 \pm 10 \mu\text{Hz}$. A value

of $\pm 10 \mu\text{Hz}$ is less than $\Delta\nu$ for all stars in our sample, and thus avoids complications due to multiple peaks in the fitting range but is also far larger than the expected frequency shifts. Visual inspection for all stars confirmed $0 \pm 10 \mu\text{Hz}$ was sufficient to allow the main peak to be fitted successfully. This process was repeated 1000 times to produce 1000 realisations of the noise. The observed $\delta\nu$ was then defined as the mean of the fitted peak locations and the uncertainty on this value, $\sigma_{\delta\nu}$, given by the standard deviation.

2.4 Determination of oscillation frequency shifts using fitted mode frequencies

The identification and characterisation of the individual mode frequencies was performed with “peakbagging” techniques. Peakbagging is the process of applying models to the power spectrum of a light curve to identify the oscillation peaks, and assigning them a value of the radial order, n , angular degree, ℓ , and azimuthal order, m (Appourchaux 2003). To perform the peakbagging of the power spectra, we used PBjam (Nielsen et al. 2021, 2025). The method of using PBjam for fitting the modes for the stars in this sample followed the same method as used in Hookway et al. (2025), and worked as follows.

PBjam performs peakbagging in two main stages, mode identification, followed by a detailed peakbagging. The mode identification began with the application of a background model to the power spectrum, with it consisting of three Harvey profiles (Harvey 1985) and a shot noise term. These terms model the instrumental variability, rotation, and magnetic activity, as well as convection on the stellar surface. The $\ell = 0, 1$ and 2 modes are characterised by the combination of Lorentzian profiles (Anderson et al. 1990), with the frequencies of the individual modes being parameterised with an asymptotic relation. There is increased complexity due to the range in evolutions for the stars in the sample. As stars evolve off the main sequence, the $\ell > 0$ modes can become mixed due to the coupling between the p- and g-mode cavities. PBjam has three models for the $\ell = 1$ modes to account for this, these being: no coupling; few g modes to many p modes; and many g modes to few p modes. For the no coupling, the asymptotic relation used for the $\ell = 2, 0$ modes is also used

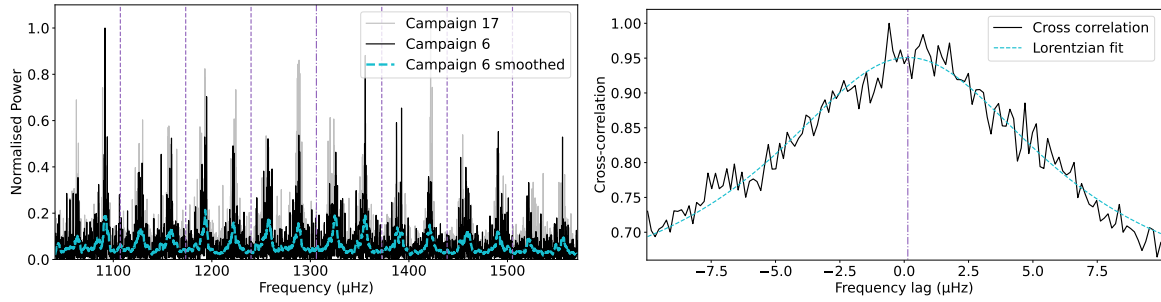


Figure 1. Left: Power spectra observed for EPIC 212509747 in campaigns 6 (black) and 17 (grey), with a smoothed version of campaign 6 (cyan dashed). Here the smoothing was performed using a boxcar of width 22 bins. The spectrum is limited to the frequency range $\nu_{\max} \pm 4\Delta\nu$. The vertical dot-dashed line indicates ν_{\max} , while the vertical dashed lines are separated from ν_{\max} by multiples of $\Delta\nu$. Right: An example of a cross-correlation (black) obtained using a realisation of the power spectra in the left panel, the Lorentzian fitted to the cross correlation (cyan, dashed) and the location of the maximum of the Lorentzian (purple, dot-dashed).

for the $\ell = 1$ modes. The other two models involve calculating the strength of the coupling between the p and g modes. PBjam does not model for mixed $\ell = 2$ modes due to the mixing of modes reducing with increasing ℓ and it becomes computationally expensive for the $\ell = 2$ modes. The posterior estimates for the asteroseismic parameters used in the models are calculated using a Bayesian framework. The prior distributions were sampled from a large dataset of thousands of previously analysed stars and stellar models to inform the mode identification posteriors. The posterior probability distributions of the model parameters were sampled using the dynesty nested sampling algorithm (Speagle 2020).

The results from the mode identification were passed to the detailed peakbagging stage of PBjam. Here, the models are largely the same as those from the mode identification stage, though now the constraints on the model parameters are relaxed. This allows for effects that would not be captured in the asymptotic relations, such as acoustic glitches and rotational splitting. The priors used on the mode frequencies were β distributions, where $\alpha = \beta = 5$ and the width of the distribution was set to half the small frequency separation, $\delta\nu_{0,2}$. Normal priors were used for the logarithmic heights and logarithmic widths, with prior widths of 50%. The posterior sampling for this stage was performed with the emcee Python library (Foreman-Mackey et al. 2013), using a Markov chain Monte Carlo algorithm. To validate the results, we computed the ratio between the median absolute deviation of the posterior distribution and the standard deviation of the prior distribution of the frequency results. If this ratio was below $2/3$, it was considered that new information on the frequency of the mode had been gained from the light curve, and the mode was retained. Those above this cut-off were removed from the analysis.

The power spectra used for the peakbagging were provided by the K2P² pipeline (Lund et al. 2015, 2024), where the pipeline reduces the effects, such as from systematic variability or potential planetary signals. The pipeline provided power spectra for the individual observational campaigns, as well as a spectrum combining the campaigns, for each star. The combined spectra were used for the mode identification. The identified modes were passed to separate detailed peakbagging analyses, where the power spectra for the individual campaigns were used.

The frequency shifts for individual modes were obtained by subtracting the frequency observed in the second campaign from the frequency observed in the first campaign. We note that this gives the frequency shifts the same sign as those determined by the cross-correlation method. For each star, a weighted average of the obtained individual mode frequency shifts was determined and taken as $\delta\nu$ for this method, with the associated weighted uncertainty giving the error $\sigma_{\delta\nu}$.

2.5 S_{ph} as a measure of magnetic activity

The above methods are based on processing the timeseries of a star to obtain the power spectrum of the data. However, another method of detecting magnetic activity in stars relies on the timeseries itself. As illustrated in Mathur et al. (2014), S_{ph} is an indicator of magnetic activity, which can be compared between stars, and is defined as the standard deviation of the timeseries. Here, S_{ph} was evaluated in the manner described in Mathur et al. (2014), applying the correction recommended by Jenkins et al. (2010) using the data supplied through the K2P² pipeline. Since these data have been cleaned for asteroseismic studies, any large deviations in the data have been removed, such as those caused by flares but the statistical noise caused by the presence of small scale active regions (such as plages, faculae, and predominantly starspots, akin to those seen on the Sun) should remain. Using helioseismic data, Salabert et al. (2017) demonstrated the S_{ph} is well correlated with solar activity proxies, such as sunspot number and Ca HK emission, while other studies (e.g. Salabert et al. 2016; Karoff et al. 2018) have shown similar agreement between S_{ph} and Ca HK emission for other stars. In Mathur et al. (2014), it was recommended to determine S_{ph} over a period corresponding to five times the rotation period of the star. This was done to negate variability in S_{ph} when determined on shorter timeseries caused by active regions coming in and out of view. Mathur et al. (2014) state that as long as S_{ph} is determined over a length of time greater than three times P_{rot} the value converges towards a constant value. In this study, we aimed to compare the activity levels in two different K2 campaigns and so, for each star, a single value of S_{ph} was determined for each campaign. Given that the typical length of a K2 campaign is around 80 d, for most stars, this is more than $3P_{\text{rot}}$ (see Table 1). For five of the stars in our sample, this is less than $3P_{\text{rot}}$ but, since longer timeseries are not available, all we can do is bear this in mind when interpreting results. We then defined a quantity called ΔS_{ph} , which was the difference between the S_{ph} values for the two campaigns and thus represents the change in activity levels. Despite the ease of this method, there are limitations to it. For the Sun, the most magnetically active regions are observed near the equator. Assuming a similar distribution of activity, if the star is inclined at an angle to our line of sight, the scatter in the timeseries will be underestimated and, hence, the result will be an underestimate of the ΔS_{ph} value.

2.6 Comparison with Kepler stars

In this work, we also aim to examine how our frequency shifts relate to various stellar parameters. As our stellar sample is small, temporal p-mode frequency shifts determined by Santos et al.

(2018) for an extensive set of Kepler stars were included for comparison. As these shifts were measured for multiple 90-day long segments in time, we must define a single value to characterise the variability of the p-mode frequency shifts. Known as the maximum frequency variation, $\delta\nu_{\max}$, this value provides an estimation for the total amplitude of frequency variation for each Kepler star.

The method to calculate $\delta\nu_{\max}$ from Santos et al. (2019) is outlined as follows. At each time point, a new shift value was randomly drawn according to a Gaussian distribution with a mean equal to the p-mode frequency shift and a standard deviation given by its uncertainty. The new values were then smoothed using a 180-day boxcar window, and the range of the resulting series was recorded. This process was repeated 10^4 times, with the median of the resulting range values taken as $\delta\nu_{\max}$ and their standard deviation as the associated uncertainty.

The $\delta\nu_{\max}$ was determined for 75 high signal-to-noise (SNR) Kepler stars, as selected by Santos et al. (2019). The authors selected stars by first calculating the SNR of the p modes in each 90-day subseries, defined as the average ratio of the mode heights of the five central orders to the background signal. They then computed the mean SNR across all subseries with a duty cycle above 70%, and retained only those targets with a final average SNR exceeding one.

It is worth noting that as Santos et al. (2018)'s temporal p-mode frequency shifts were calculated relative to a reference segment, we do not know where in the magnetic activity cycle we view or how much of it we observe. Without repeated observations covering the full activity cycle, the true maximum frequency shift for each star cannot be determined. The $\delta\nu_{\max}$ may, therefore, underestimate the total amplitude of frequency variation.

Frequency shifts determined by this work, along with $\delta\nu_{\max}$ for the 75 high-SNR Kepler stars, were compared to stellar parameters. The results of which are presented in Section 3. Except for $\log \Delta S_{\text{ph}}$, whose calculation is described prior, the stellar parameters equivalent to those described in Section 2.2, for the stars from the high-SNR Kepler stars can be found in Santos et al. (2018) and references therein.

3 Results and Discussion

3.1 Observed frequency shifts

Table 2 shows the observed $\delta\nu$ for each star using the cross-correlation method and the fitted mode frequencies. Figure 2 shows a comparison between the frequency shifts obtained with the two methods. There is no clear one-to-one trend. However, this was not entirely unexpected given that the frequency shifts were generally small compared to their uncertainties and we note that the difference in the obtained frequency shift by the two methods was less than 1.1σ for all stars, demonstrating broad agreement. We note that, in agreement with previous studies, the errors associated with the frequency shifts determined using the fitted frequencies were smaller than those obtained from cross correlations. As can be seen in Table 2, no frequency shifts were obtained using the fitted frequencies for EPIC 212617037. This was because no modes passed the fitted validation test in either campaign, indicating a low confidence in the validity of the fitted frequencies, with the power spectrum not being able to provide sufficient new information on the mode compared to the prior.

Three stars exhibit $\delta\nu > \sigma_{\delta\nu}$ when using both the cross-correlation method and the fitted frequencies (EPICs 212478598, 212509747 and 246134147). A further two stars (EPIC 246033065 and EPIC 246438837) exhibit $\delta\nu > \sigma_{\delta\nu}$ when using the cross-correlation method but not the fitted frequencies, while two stars (EPIC 212516207 and EPIC 246305274) were

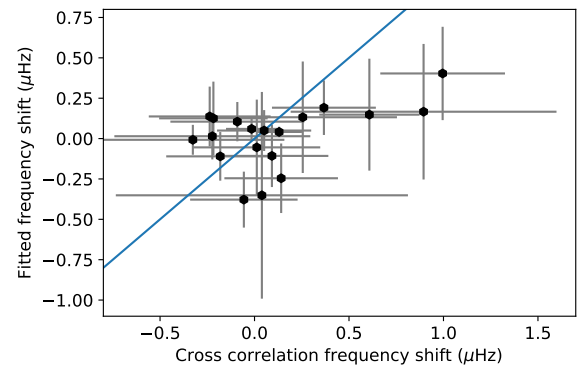


Figure 2. Comparison of the frequency shifts obtained using cross correlations and the fitted frequencies (data points). A 1:1 line is included for guidance.

found to have $\delta\nu > \sigma_{\delta\nu}$ when using the fitted frequencies but not the cross-correlation method. Therefore, seven stars in total exhibit $\delta\nu > \sigma_{\delta\nu}$ for at least one method. For the remaining 13 stars, $\delta\nu < \sigma_{\delta\nu}$ for both methods.

González-Cuesta et al. (2023) studied eight stars, all of which are in our sample, observed in campaigns 6 and 17. These stars are highlighted using an asterisk or dagger symbol in Table 2. González-Cuesta et al. did not look for evidence of frequency shifts in EPIC 212478598 and EPIC 212683142 (highlighted using the dagger symbol), since they are sub-dwarfs and therefore are not expected to be magnetically active. However, given the results of Kiefer et al. (2019), which suggest that even a small change in the magnetic field could produce noticeable frequency shifts in evolved stars, we left these stars in our sample. We note that EPIC 212478598 was one of the stars in our sample that showed a $\delta\nu > \sigma_{\delta\nu}$ in both methods (while EPIC 212683142 shows no evidence for a frequency shift). González-Cuesta et al. (2023) found no evidence of frequency shifts in the remaining six stars. These stars are highlighted by asterisks in Table 2, where it can be seen that we found no evidence of a frequency shift for four of the stars but did find $\delta\nu > \sigma_{\delta\nu}$ (the same criteria as considered by González-Cuesta et al.) for two stars: EPIC 212509747 (using both methods) and EPIC 212516207 (using the fitted frequencies only). Although González-Cuesta et al. also used fitted frequencies to determine whether there were frequency shifts, they used a different fitting code and time series preparation techniques, which may have contributed to this discrepancy.

The fact that the frequency shifts are relatively small for the majority of stars is somewhat expected, given that the difference in time between two overlapping campaigns is relatively small. The start dates of campaigns 16 and 18 are separated by 156 days, the start dates of campaigns 6 and 17 are separated by 961 days, and the start dates of campaigns 12 and 19 are separated by 622 days. These are all relatively short time frames compared to the Sun's approximately 11 yr magnetic activity cycle.

Even if a star exhibits an activity cycle, there are various factors that would determine whether we would see evidence for that cycle within the data. For instance, the lengths of stellar cycles are typically of the order of years (Baliunas et al. 1995). While the length of a cycle is observed to increase with increasing rotation period (e.g. Metcalfe & van Saders 2017, and references therein), there is still a large amount of scatter in this relation. The reason for this the scatter is still not well understood (see Jeffers et al. 2023, for a recent review), making it difficult to predict, a priori, what the length of a cycle for a star will be. It is also worth noting that within the Mount Wilson sample, only around 50 per cent of observed stars showed evidence for activity cycle-like behaviour, with a further ~ 25 per cent showing more chaotic variability

Table 2. Frequency shifts ($\delta\nu$) obtained by two different methods: “Cross” refers to those frequency shifts obtained from the cross correlation and n_{sm} gives the number of bins smoothed over before creating the 1000 realisations; “Fitted” refers to the frequency shifts obtained using the fitted mode frequencies. Also included in the table are details of which K2 campaigns were used for each star and $\log \Delta S_{\text{ph}}$, which is a proxy for the change in magnetic activity between the two campaigns. An asterisk indicates that [González-Cuesta et al. \(2023\)](#) found no evidence of a frequency shift for these stars, while a dagger indicates that the stars were in the sample of [González-Cuesta et al. \(2023\)](#) but that they did not determine whether any frequency shift was observed.

EPIC	Campaign		Frequency shift (μHz)		n_{sm}	$\log \Delta S_{\text{ph}}$
	1	2	Cross	Fitted		
$\delta\nu < \sigma_{\delta\nu}$						
211403248	16	18	-0.1 ± 0.4	0.10 ± 0.12	7	2.95
211409560	16	18	-0.2 ± 0.5	0.01 ± 0.14	6	2.75
212485100*	6	17	-0.18 ± 0.29	-0.11 ± 0.15	29	3.17
212487676*	6	17	0.0 ± 0.2	0.05 ± 0.13	26	1.83
212617037*	6	17	0.1 ± 0.5	–	17	1.76
212683142 [†]	6	17	-0.02 ± 0.14	0.06 ± 0.08	15	2.55
212708252	6	17	-0.3 ± 0.5	-0.01 ± 0.09	45	2.19
212709737	6	17	0.0 ± 0.8	-0.4 ± 0.6	26	1.83
212772187*	6	17	0.3 ± 0.5	0.1 ± 0.3	30	2.46
245961434	12	19	-0.2 ± 0.3	0.14 ± 0.18	16	2.94
245972483	12	19	-0.2 ± 0.3	0.12 ± 0.23	28	3.10
246154489	12	19	0.1 ± 0.3	-0.11 ± 0.19	5	2.15
246212144	12	19	0.0 ± 0.3	0.0 ± 0.3	18	2.36
$\delta\nu > \sigma_{\delta\nu}$, both methods						
212478598 [†]	6	17	0.13 ± 0.12	0.04 ± 0.03	11	1.06
212509747*	6	17	0.4 ± 0.3	0.19 ± 0.17	22	2.33
246143147	12	19	1.0 ± 0.3	0.4 ± 0.3	28	3.39
$\delta\nu > \sigma_{\delta\nu}$, cross only						
246033065	12	19	0.9 ± 0.7	0.2 ± 0.4	35	2.78
246438837	12	19	0.6 ± 0.3	0.1 ± 0.3	18	3.09
$\delta\nu > \sigma_{\delta\nu}$, fitted only						
212516207*	6	17	-0.1 ± 0.3	-0.38 ± 0.17	23	2.32
246305274	12	19	0.1 ± 0.3	-0.25 ± 0.22	16	2.48

in activity and ~ 25 per cent showing little to no variability in activity whatsoever ([Baliunas et al. 1995](#)). Furthermore, the phase of the cycle when the observations take place will impact the magnitude of any frequency shift. Ideally, the observations would take place at the start and end of a rising or falling phase of a cycle, respectively, to maximise the frequency shift. However, we are just as likely to make two observations at around cycle maximum or minimum, when the difference in frequency would be minimal. Any frequency shifts observed here can, therefore, be considered as a minimum for the cycle amplitude.

3.2 Dependence of frequency shifts on stellar parameters

Figure 3 demonstrates how the observed frequency shifts vary with different stellar parameters. For comparison, we have also included the results from [Santos et al. \(2019\)](#). Table 3 gives the Spearman’s rank correlation ρ_{sp} and corresponding p values between the frequency shifts and stellar parameters. These were computed using just the K2 frequency shifts and by combining with the Kepler results from [Santos et al. \(2019\)](#) (and as described in Section 2.6).

The top left panel of Figure 3 shows the variation in frequency shift with $\Delta\nu$. It can be seen that our sample extends to lower $\Delta\nu$ values than considered by [Santos et al. \(2019\)](#), as their sample only contained main-sequence stars, whereas ours also contains some subgiant stars. Only one of these evolved stars exhibits frequency shifts larger than their errors. We note that the range of frequency shifts observed is consistent with those seen by [Santos et al.](#), however, the error bars are noticeably larger for the K2 stars. This

is likely due to additional noise present in the K2 data compared to the more stable Kepler data. No noticeable trend was observed between $\Delta\nu$ and $\delta\nu$, and the ρ_{sp} values were not significant (see Table 3). However, we note that although our sample of stars with $\delta\nu > \sigma_{\delta\nu}$ is only small, the magnitude of the shift for those stars appears to generally increase with $\Delta\nu$.

The top right panel of Figure 3 shows the variation in $\delta\nu$ with effective temperature, T_{eff} . [Santos et al.](#) observed a positive correlation (Spearman’s rank of 0.68) between the frequency shifts and T_{eff} . When considering the frequency shifts obtained using the cross-correlation method, no such correlation was observed, and the observed ρ_{sp} was not significant when using only the K2 data. When combined with the Kepler results, the value of ρ_{sp} was significant, but lower than that observed by [Santos et al.](#), reflecting the fact that no correlation was observed in the K2 data. However, when the fitted frequencies were used to determine $\delta\nu$ a value of $\rho_{\text{sp}} = 0.678$ was observed for just the K2 data, which was significant at a 1 per cent level. When combined with the Kepler data, the value of ρ_{sp} decreased to 0.562 but is more significant, due to the substantial increase in the number of data points.

The middle left panel of Figure 3 shows how the frequency shift varies with surface gravity ($\log g$). This result again highlights the fact that the larger shifts in our sample were observed for the main-sequence stars (those with higher $\log g$ values), while the majority of evolved stars show shifts consistent with zero. Although [Santos et al. \(2019\)](#) did not plot the variation in $\delta\nu$ as a function of $\log g$, it can be seen from Figure 3 that our sample consists of a wider range of $\log g$ values (because of the presence of subgiants). As can be seen from Figure 3, the largest

Table 3. Spearman’s rank correlations (ρ_{sp}) and corresponding p values between the observed frequency shifts, obtained using the cross-correlation (Cross) method and the fitted mode frequencies (Fitted) and various stellar parameters. Correlation coefficients were obtained using the frequency shifts obtained from the K2 data only (K2) and from the combined K2 and Kepler frequency shifts (from Santos et al. 2019, and Section 2.6).

	K2 only				K2 and Kepler			
	Cross		Fitted		Cross		Fitted	
	ρ_{sp}	p value	ρ_{sp}	p value	ρ_{sp}	p value	ρ_{sp}	p value
$\Delta\nu$	0.421	0.065	0.257	0.286	0.112	0.395	0.059	0.655
T_{eff}	0.120	0.613	0.678	0.001	0.431	5×10^{-4}	0.562	3×10^{-6}
$\log g$	0.395	0.084	0.254	0.293	0.137	0.296	0.084	0.525
[Fe/H]	0.117	0.622	0.146	0.552	0.230	0.076	0.305	0.019
P_{rot}	-0.250	0.289	-0.600	0.007	-0.462	0.001	-0.605	8×10^{-6}
$\log \Delta S_{\text{ph}}$	0.347	0.133	0.356	0.135	-0.168	0.198	-0.315	0.015

shifts in our sample were observed for stars with $\log g \approx 4.2$, which is broadly in agreement with the results of Santos et al. as plotted here. No significant correlation was observed between the frequency shifts and $\log g$.

The middle right panel shows frequency as a function of metallicity ([Fe/H]). While Santos et al. found no significant correlation with metallicity, they did find tentative evidence for two sequences. Again, our results are consistent with this. No significant correlations were observed (see Table 3) but we note the presence of stars with shifts larger than their errors populating the upper sequence identified by Santos et al.

The bottom left panel shows the variation in frequency shift with surface rotation period. Santos et al. found a negative Spearman’s rank correlation of -0.61 between these two parameters. Our results are consistent with this trend, with the stars that show the largest shifts, i.e. those with $\delta\nu > \sigma_{\delta\nu}$, also being relatively fast rotators. The agreement between these stars and those from Santos et al. (2019) can be seen more clearly in the inset figure, which focuses on the faster rotating stars in the sample. We note that some of the fast rotators had frequency shifts consistent with zero. However, as mentioned previously, this may simply be because the time separation of the overlapping campaigns was not large enough. Similarly, those campaigns may coincide with either a maximum or minimum phase in an activity cycle, in which case, the frequencies would remain approximately constant. Table 3 demonstrates that while ρ_{sp} was found to be negative when considering the K2 frequency shifts obtained using the cross-correlation method, this correlation was not significant, likely due to the frequency shifts on fast rotators being consistent with zero. However, when using the frequency shifts obtained from the fitted frequencies, $\rho_{\text{sp}} = -0.600$, which was significant at a 1 per cent level. Our sample spans a wider range of rotation rates than Santos et al., again reflecting the fact that our sample contains subgiant stars. Our results demonstrate that the expected decrease in frequency shift, and thus by inference magnetic activity, with increasing rotation period extends to higher rotation rates than previously studied.

The bottom right panel shows the variation in frequency shift with $\log \Delta S_{\text{ph}}$. While no significant correlation was observed (see Table 3), it is worth pointing out that those stars with the largest frequency shifts also have relatively large values of $\log \Delta S_{\text{ph}}$. However, it is interesting to note that the sign of the correlation changed from positive when only the K2 data were used to negative when the K2 data were combined with the Kepler data. An outlier in this sample is the evolved star (EPIC 212478598), which shows a small frequency shift, but one that is greater than its error bars, and also by far the lowest variation in S_{ph} .

Figure 4 shows how the non-absolute values of frequency shift vary with S_{ph} . Spearman’s rank correlation coefficient between these two variables was found to be $\rho_{\text{sp}} = 0.37$, with a corresponding p value of 0.1, when the cross-correlation frequency

shifts were used, and $\rho_{\text{sp}} = 0.5$, with a p value of 0.03, when the fitted frequency shifts were used. This suggests that there may be a weak correlation, but that the correlation is not significant. This is not entirely surprising given the large number of stars without significant frequency shifts. However, we note that the three stars with large positive frequency shifts found using the cross-correlation method also have large positive changes in ΔS_{ph} .

4 Conclusions

We have searched for evidence for variations in asteroseismic p-mode frequencies in stars observed by the K2 mission in two different time-separated campaigns. We used the KEYSTONE asteroseismic sample (Lund et al. 2024) to identify candidates with previously observed p modes and further used the time series optimised for asteroseismology by that study. Our sample consisted of 20 main-sequence and subgiant stars. We used two methods to determine whether any average change in frequency (known as a frequency shift, $\delta\nu$) existed, namely a cross-correlation method and one based on fitting the observed power spectra to determine the individual frequencies of the modes. Out of these 20 stars, seven stars were found to have frequency shifts larger than the associated errors ($\delta\nu > \sigma_{\delta\nu}$) in total: three using both methods; two using the cross-correlation method only, and a different two using the fitted frequencies only. It was not surprising that the majority of stars did not show evidence for a frequency shift, given uncertainties over cycle lengths, amplitudes and phases or even whether a star is likely to exhibit a cycle at all. However, it would be useful to monitor the stars that show some evidence of frequency shifts in the future to determine if they really do have observable magnetic activity cycles. Of particular note is EPIC 212478598, which is a sub-giant star that exhibited $\delta\nu > \sigma_{\delta\nu}$ using both methods. Evolved stars are not expected to be magnetically active, and indeed, this star has a very low $\log(\Delta S_{\text{ph}})$ value but the fact that its frequencies appear to change, hints at the fact that some magnetic variability may remain, even if hidden beneath the surface (where it could impact the p modes, without causing variations in S_{ph}). This result motivates future studies of evolved stars with visible solar-like oscillations, such as those observed with Kepler, which have been neglected by previous studies.

When comparing the observed frequency shifts with stellar parameters, our results are in broad agreement with the results obtained by Santos et al. (2019) using Kepler stars. In particular, larger frequency shifts were observed for stars with shorter rotation periods, which likely reflects the fact that these stars are expected to be more magnetically active, and, importantly, have shorter activity cycles (Metcalf & van Saders 2017). A significant positive correlation was observed between the frequency shifts obtained using the fitted frequencies and T_{eff} , which is

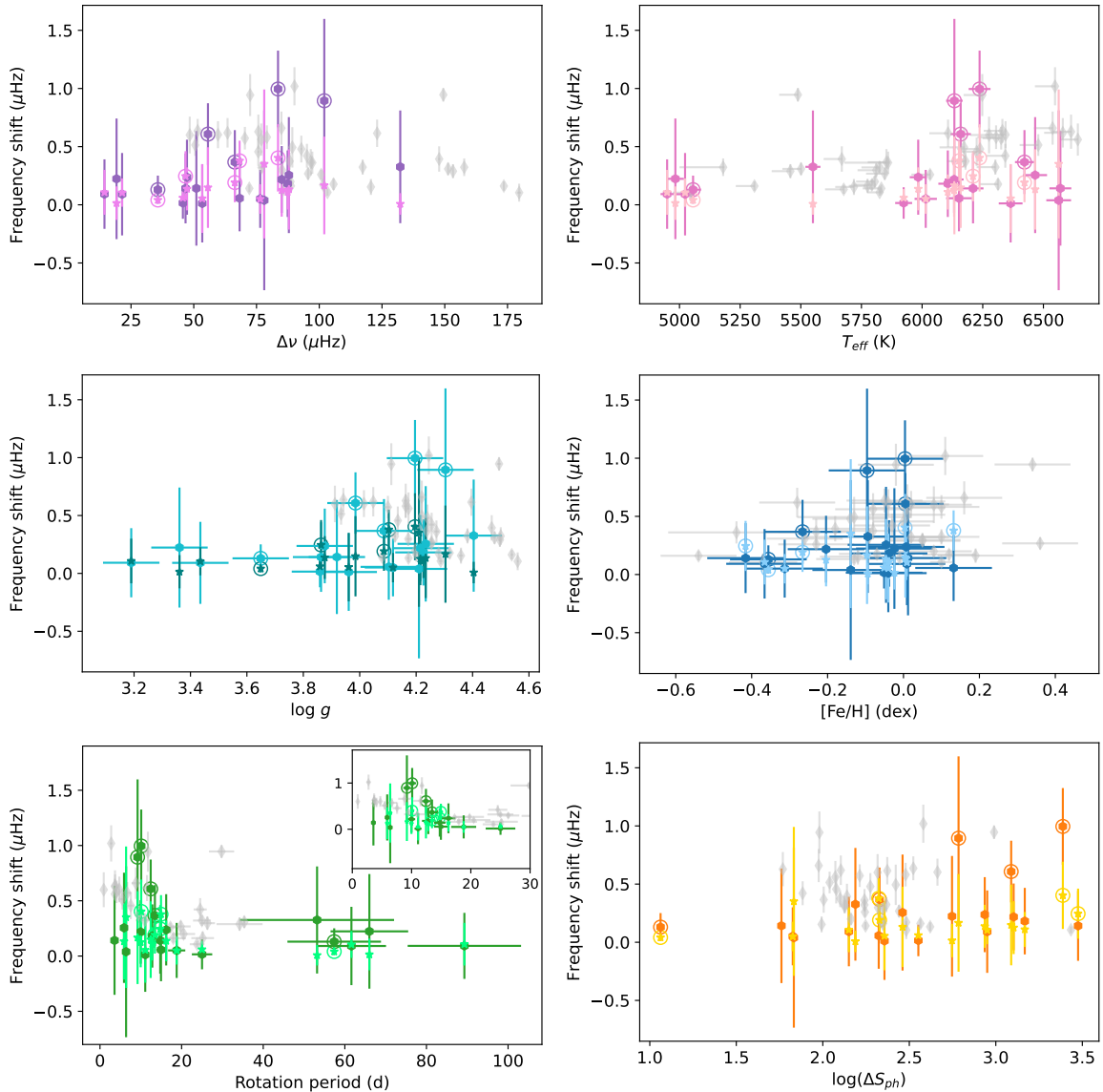


Figure 3. Variation in frequency shift with different stellar parameters. In all figures, the hexagon symbols denote results obtained using the cross-correlation method, while the star symbols denote results obtained using the fitted frequencies. Open circles highlight those stars where the observed shift was larger than the uncertainty. All frequency shifts are the absolute values since it is the magnitude of the shift that is important, not whether the frequencies have increased or decreased between campaigns. The grey data were based on the results of Santos et al. (2019). Top left: Large frequency separation, $\Delta\nu$. Top right: Effective temperature, T_{eff} . Middle left: Surface gravity, $\log g$. Middle right: Metallicity ($[\text{Fe}/\text{H}]$). Bottom left: $\log \Delta S_{\text{ph}}$. Bottom right: Rotation period, P_{rot} , where the inset focuses on the faster rotating stars in our sample.

again in agreement with Santos et al.. There does appear to be some sensitivity in the amplitude of $\delta\nu$ with $\log g$, but no significant correlation was observed. The dependence of the frequency shifts on T_{eff} (and potentially $\log g$) may relate to sensitivity of the modes to a perturbation as predicted by Metcalfe et al. (2007); Kiefer et al. (2019); Kiefer & Broomhall (2020). The dependence of $\delta\nu$ on $[\text{Fe}/\text{H}]$ was consistent with the presence of two branches, as highlighted by Santos et al. (2019). Similarly, no clear trend was observed between $|\delta\nu|$ and $\log(\Delta S_{\text{ph}})$, while only a weak correlation was found between $\delta\nu$ and ΔS_{ph} (i.e. accounting for the sign of any change).

The results of this paper highlight the need to increase the number of stars for which we can obtain frequency shifts so as to better understand stellar activity cycles. When observing a star only twice, there is no guarantee that, even if an activity cycle exists, the magnetic activity levels at the times of observation will be different. The observed frequency shift, therefore, will represent a lower limit on the frequency shift between cycle min-

imum and maximum. We therefore need a larger number of stars to fully understand how stellar parameters impact activity cycles. Furthermore, dedicated long-term monitoring of stars with known frequency variations is needed to determine whether the observed frequency shifts are due to cycles or more chaotic magnetic activity. For these stars in particular, the K2 results could be combined with longer term monitoring to add to our current database of stars with activity cycles and to help our understanding of solar and stellar dynamos.

Acknowledgements

GB wishes to thank Dr. Valentina Ekimova (University of Virginia) and Charlotte Pettett (University of Warwick) for their aid with this research and publication. GB and AMB acknowledge the support of the Undergraduate Research Support Scheme (URSS) offered by Warwick University and the Royal Astronomical Society grant for undergraduate research. AMB, DYK

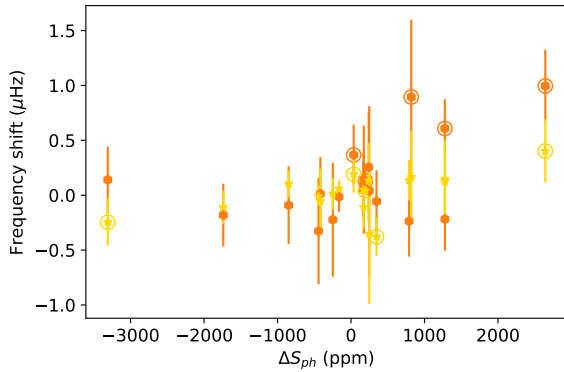


Figure 4. Variation in frequency shift with ΔS_{ph} . The hexagon symbols denote results obtained using the cross-correlation method, while the star symbols denote results obtained using the fitted frequencies. Open circles highlight those stars where the observed shift was larger than the uncertainties.

and LJM acknowledge support from the Science and Technology Facilities Council (STFC) grant No. ST/X000915/1 and ST/T000252/1. DYK also acknowledge the Latvian Council of Science Project No. lzp2022/1-0017. LJM gratefully acknowledges support from the UK Science and Technology Facilities Council (STFC) grant ST/W507908/1. MNL acknowledges support from the ESA PRODEX programme.

This study also acknowledges use of Python packages NumPy (Harris et al. 2020), Matplotlib (Hunter 2007), and SciPy (Virtanen 2020). This work also made use of AstroPy, a community-developed core Python package and an ecosystem of tools and resources for astronomy (Astropy Collaboration 2013, 2018, 2022).

Data Availability

K2 KEYSTONE data available upon request to MNL.

REFERENCES

- Anderson E. R., Duvall Jr. T. L., Jefferies S. M., 1990, *ApJ*, **364**, 699
 Appourchaux T., 2003, *Ap&SS*, **284**, 109
 Astropy Collaboration 2013, *Astronomy and Astrophysics*, **558**, A33
 Astropy Collaboration 2018, *The Astronomical Journal*, **156**, 123
 Astropy Collaboration 2022, *Astrophysical Journal*, **935**, 167
 Baliunas S. L., et al., 1995, *ApJ*, **438**, 269
 Balogh A., Thompson M. J., 2009, *Introduction to Solar Magnetism: The Early Years*. Springer New York, New York, NY, pp 1–14, doi:10.1007/978-1-4419-0239-9_1, https://doi.org/10.1007/978-1-4419-0239-9_1
 Bell K. J., Hekker S., Kuszlewicz J. S., 2019, *MNRAS*, **482**, 616
 Borucki W. J., et al., 2010, *Science*, **327**, 977
 Broomhall A.-M., Chatterjee P., Howe R., Norton A., Thompson M., 2014, *Space Science Reviews*, **186**, 191
 Charbonneau P., 2014, *Annual Review of Astronomy and Astrophysics*, **52**, 251
 Dziembowski W. A., Goode P. R., 2005, *The Astrophysical Journal*, **625**, 548
 Elsworth Y., Howe R., Isaak G. R., McLeod C. P., New R., 1990, *Nature*, **345**, 322
 Ferreira R. R., Gonçalves B. F. O., do Nascimento J. D., Castro M., 2024, *MNRAS*, **535**, 2394
 Foreman-Mackey D., Hogg D. W., Lang D., Goodman J., 2013, *Publications of the Astronomical Society of the Pacific*, **125**, 306–312
 García R. A., Ballot J., 2019, *Living Reviews in Solar Physics*, **16**, 4
 García R. A., Mathur S., Salabert D., Ballot J., Régulo C., Metcalfe T. S., Baglin A., 2010, *Science*, **329**, 1032
 González-Cuesta L., et al., 2023, *A&A*, **674**, A106

- Hale G. E., 1908, *ApJ*, **28**, 315
 Handberg R., Lund M. N., 2014, *MNRAS*, **445**, 2698
 Harris C. R., et al., 2020, *Nature*, **585**, 357
 Harvey J., 1985, in Rolfe E., Battrick B., eds, *ESA Special Publication Vol. 235, Future Missions in Solar, Heliospheric & Space Plasma Physics*, p. 199
 Hathaway D. H., 2015, *Living Reviews in Solar Physics*, **12**, 4
 Hookway G. T., Nielsen M. B., Davies G. R., Lund M. N., García R. A., Mathur S., See V., Stokholm A., 2025, *Peakbagging the K2 KEYSTONE sample with PBjam: characterising the individual mode frequencies in solar-like oscillators (arXiv:2510.21626)*, https://arxiv.org/abs/2510.21626
 Howell S. B., et al., 2014, *PASP*, **126**, 398
 Hunter J. D., 2007, *Computing in Science & Engineering*, **9**, 90
 Jeffers S. V., Kiefer R., Metcalfe T. S., 2023, *Space Sci. Rev.*, **219**, 54
 Jenkins J. M., et al., 2010, *ApJ*, **713**, L120
 Karoff C., et al., 2018, *ApJ*, **852**, 46
 Kiefer R., Broomhall A.-M., 2020, *MNRAS*, **496**, 4593
 Kiefer R., Roth M., 2018, *ApJ*, **854**, 74
 Kiefer R., Schad A., Davies G., Roth M., 2017, *A&A*, **598**, A77
 Kiefer R., Broomhall A.-M., Ball W. H., 2019, *Frontiers in Astronomy and Space Sciences*, **6**, 52
 Kjeldsen H., et al., 2025, *A&A*, **700**, A39
 Kolotkov D. Y., Broomhall A.-M., Hasanzadeh A., 2024, *MNRAS*, **533**, 3387
 Lund M. N., Handberg R., Davies G. R., Chaplin W. J., Jones C. D., 2015, *ApJ*, **806**, 30
 Lund M. N., et al., 2024, *A&A*, **688**, A13
 Mamajek E. E., Hillenbrand L. A., 2008, *ApJ*, **687**, 1264
 Mathur S., et al., 2014, *A&A*, **562**, A124
 Maunder E. W., 1904, *MNRAS*, **64**, 747
 Metcalfe T. S., van Saders J., 2017, *Sol. Phys.*, **292**, 126
 Metcalfe T. S., Dziembowski W. A., Judge P. G., Snow M., 2007, *MNRAS*, **379**, L16
 Nielsen M. B., et al., 2021, *The Astronomical Journal*, **161**, 62
 Nielsen M. B., et al., 2025, *The Astronomical Journal*, **169**, 322
 Salabert D., et al., 2016, *A&A*, **589**, A118
 Salabert D., García R. A., Jiménez A., Bertello L., Corsaro E., Pallé P. L., 2017, *A&A*, **608**, A87
 Santos A., et al., 2018, *The Astrophysical Journal Supplement Series*, **237**, 17
 Santos A., et al., 2019, *The Astrophysical Journal*, **883**, 65
 Schwabe H., 1844, *Astronomische Nachrichten*, **21**, 233
 Skumanich A., 1972, *ApJ*, **171**, 565
 Speagle J. S., 2020, *Monthly Notices of the Royal Astronomical Society*, **493**, 3132–3158
 Virtanen P., 2020, *Nature Methods*, **17**, 261
 Woodard M. F., Noyes R. W., 1985, *Nature*, **318**, 449

This paper has been typeset from a $\text{\TeX}/\text{\LaTeX}$ file prepared by the author.